Pharm Res (2015) 32:2086–2096
DOI 10.1007/s11095-014-1601-2

RESEARCH PAPER

Multi-Scale Modelling of Powder Dispersion in a Carrier-Based Inhalation System

Zhenbo Tong • Hidehiro Kamiya • Aibing Yu • Hak-Kim Chan • Runyu Yang

Received: 8 October 2014 / Accepted: 8 December 2014 / Published online: 17 December 2014

ABSTRACT

Purpose Carrier-based dry powder inhalers (DPIs) are widely used for rapid and convenient delivery of drug to the site of action. This work aimed to predict powder aerosolisation in DPIs through numerical modelling.

Methods A multi-scale modelling technique based on the combined computational fluid dynamics (CFD) and discrete element method (DEM) approach was developed.

Results The simulation results of the detachments of the drug particles from single carrier under different impact velocities and angles were comparable with those measured in the experiments in terms of fine particle fraction FPF_{loaded}. Empirical equations were developed to link the detachment performance with impact velocity and impact angle. Then the dynamics of the carrier particles in Aerolizer® was simulated. The results indicated that the carrier-wall impaction was the dominant mechanism for drug aerosolisation performance. By linking the empirical equations with the carrier-wall impact energy, the predictions showed that for a given formulation mass with a fixed carrier/drug ratio, the inhaler performance decreased with carrier size and increased with air flow rate. Device empty efficiency, however, was independent with carrier size and flow rate.

Conclusions The multi-scale model was able to provide quantitative information to better understand the aerosolisation mechanisms of carrier-based formulation.

KEY WORDS carrier-based formulation · computational fluid dynamics · discrete element method · dry powder inhaler · numerical modelling · powder dispersion

INTRODUCTION

Inhalation aerosols offer the distinct advantage of rapid and convenient delivery of bioactive substances to the site of action (1–3). Recently significant research effort has been directed towards the development of innovative technologies for the generation and delivery of dry powder aerosols for inhalation (4,5). Compared with other inhalation technologies, dry powder aerosols require no propellant, have superior chemical stability, better bacterial growth resistance and are also easy to use.

Successful delivery of a drug to the lungs can only be achieved by a combination of inhaler device, drug formulation and inhalatory manoeuvre capable of producing an aerosol of drug particles with an aerodynamic diameter smaller than 5 μm (6). Particles of this size have strong inter-particle cohesion with poor flowability, making powder device filling and aerosolisation difficult. The most common solution to these problems is to blend fine respirable drug particles with coarser particles of an inert excipient (usually lactose) carrier (7,8). The so-called carrier-based DPI formulations enable the fine drug particles to adhere to the surface of the coarse carrier particles (9). Upon aerosolisation, the drug particles are liberated from the carrier and delivered into the respiratory tree while the carriers impact in the oropharynx and are swallowed.

Extensive research has been carried out to improve the aeroionisation performance by controlling the roughness (10,11), shape (10), surface energy (12), size (5,13–15) and size distribution (16) of carriers, the drug/carrier ratio (17–20), fine

Z. Tong • H. Kamiya
Graduate School of Bio-Applications and Systems Engineering (BASE)
Tokyo University of Agriculture and Technology,
Koganei, 184-8588 Tokyo, Japan

Z. Tong • A. Yu • R. Yang (✉)
School of Materials Science and Engineering University of New South Wales, Sydney, NSW 2052 Australia
e-mail: r.yang@unsw.edu.au

A. Yu
Department of Chemical Engineering Monash University, Clayton 3900 Australia

H.-K. Chan
Faculty of Pharmacy University of Sydney, Sydney, NSW 2006, Australia

excipient particles (21) and charge (22,23). However, present pharmaceutical dry powder inhalers (DPIs) are extremely inefficient (only 10–30% of the stated dose reaches the lungs), leading to an undesirable large variability of dosing (3,24). The mechanism of drug–carrier blend formation and drug liberation during powder fluidisation/aerosolisation is still poorly understood, mainly due to the difficulty in obtaining detailed information from experiments. This has become a major obstacle to further improving inhaler performance. Numerical modelling has been used to investigate the powder dispersion in inhalers and to generate more detailed information at the microscopic level (25–28). Computational fluid dynamics (CFD) models have been adopted to investigate the effect of design on the performance of DPIs (25,26). CFD models also were combined with the discrete element method (DEM) to model the air flow in agglomerate-based aerosolisation in DPIs (29). More recently, Yang *et al.* (30) conducted a CFD-DEM study to investigate the effect of air flow on the detachment of powders from carriers. However, there has been no study to simulate powder dispersion in carrier-based DPIs.

Modelling such a system represents a significant challenge for the CFD-DEM based simulations. In addition to a large number of fine powders involved in the system, the size ratio between carrier particles and drug particles can be over 50, which makes the direct simulation of the system computationally very difficult if not impossible. To overcome such problem, this paper is to propose a multi-scale approach based on an assumption that the powder dispersion in an inhaler depends on the "detachment behaviour" of fine drug powders from carriers and "energy environment" inside the inhaler. The former depends on the characteristics and material properties of carrier and drug particles, and the latter depends of the device design and operation conditions. By linking this information, the overall aerosolisation performance of the inhaler will be predicted.

NUMERICAL MODEL AND SIMULATION CONDITIONS

CFD-DEM Model

The detailed description of the CFD-DEM model was given previously (28) and is summarised here. By treating the dispersion process as a particle-fluid flow, the discrete particles and the continuous air flow are modelled by the DEM and CFD, respectively. In the DEM model, the motions of a particle (of mass m_i and radius R_i) are governed by Newton's second law of motion (31), given by

$$m_i\frac{\mathrm{d}\mathbf{v}_i}{\mathrm{d}t} = \mathbf{f}_{pp,i} + \mathbf{f}_{pf,i} + m_i\mathbf{g} \tag{1}$$

$$I_i\frac{\mathrm{d}\boldsymbol{\omega}_i}{\mathrm{d}t} = \mathbf{T}_i \tag{2}$$

where m_i , I_i, $\mathbf{v}_i$, and $\boldsymbol{\omega}_i$ are, respectively, the mass, moment of inertia, translational and rotational velocities of particle i. coefficient. The inter-particle forces $\mathbf{f}_{pp,i}$ include the contact force, damping force and the van der Waals force. Other forces are the particle-fluid interaction force $\mathbf{f}_{pf,i}$ and gravity. $\mathbf{T}_i$ is the total torque acting on the particle.

The motion of fluid in CFD model is governed by the Navier–Stokes equations, given by (32,33)

$$\frac{\partial\varepsilon}{\partial t} + \nabla\cdot\left(\varepsilon\overline{\mathbf{u}}\right) = 0 \tag{3}$$

$$\frac{\partial\left(\rho_f\varepsilon\overline{\mathbf{u}}\right)}{\partial t} + \nabla\cdot\left(\rho_f\varepsilon\overline{\mathbf{u}}\overline{\mathbf{u}}\right) = -\nabla P - \mathbf{F}_{fp} + \nabla\cdot(\varepsilon\boldsymbol{\tau}) + \rho_f\varepsilon\mathbf{g} + \nabla\cdot\left(-\rho\overline{\mathbf{u}'\mathbf{u}'}\right) \tag{4}$$

where ε, $\bar{\mathbf{u}}$, $\mathbf{u}'$, ρ_f, P and $\boldsymbol{\tau}$ are porosity, fluid mean velocity, turbulent velocity fluctuation, fluid density, pressure and fluid viscous stress tensor, respectively. The volumetric fluid-particles interaction force $\mathbf{F}_{fp}$ is the summation of the particle-fluid interaction $\mathbf{f}_{pf}$ acting on all the particles in a CFD cell (33). In the study, the Reynolds numbers range from 6.4×10^4 to 10^5, indicating the flow inside the inhaler is a typical turbulent flow. The Reynolds stress model (RSM) was therefore adopted for turbulence as it provides a better description of the swirl flow (34,35). The normalized Reynolds stress residuals in the range of 10^{-4} have been applied as the convergence criteria to ensure full convergence.

A two way CFD-DEM coupling method was adopted in the study. The coupling was achieved by combining the DEM code with commercial CFD software Fluent® through its User Defined Functions (UDFs). Various functions were implemented in the UDF which can be roughly categorized into two groups: (i) the functions to simulate particle movements in the DEM; and (ii) the functions to transfer the data between the DEM and CFD. At each time step, based on fluid flow field, the DEM simulation calculated particle-related information based on fluid flow field, such as the positions and velocities of individual particles, to determine porosity and volumetric particle-fluid interaction force in the individual computational cells. CFD then used these data to determine the air flow field which then yields the particle-fluid interaction forces acting on individual particles. Incorporation of the resulting forces into the DEM produced information about the motion of individual particles for the next time step, and the process continued.

Simulation Conditions

The powder dispersion in a commercial inhaler, Aerolizer®, was simulated. The inhalation system was used in our previous study on the dispersion of a carrier free system (29). Figure 1 shows its geometry and the corresponding mesh. The inhaler

consists of a chamber with two inlets, a barrel, a grid in between and a capsule for powder storage. The mesh sizes between 0.15 mm-0.2 mm were used in the current study, which was the same as those used in our previous work (29). It was demonstrated (29) that the mesh independence in terms of the fluid field and particle flow was achieved with the selected mesh sizes. It is also suggested that the mesh size in the CFD-DEM model should be at least 1.5–2 times particle size. The current mesh sizes therefore met the requirement compared with the size of carrier particles (70–130 μm). The total number of mesh elements in the simulations was 691,561. Both unstructured (tetrahedral) and structured (hexahedron) meshes were used and the structured meshes were preferred wherever possible (e.g. the barrel).

The carrier based formulation was obtained by mixing carrier particles (lactose) with fine drug particles (mannitol). While the carrier particles had a size distribution from 70 to 130 μm, the drug particles were mono-sized at 2 μm. The drug/carrier mass ratio was fixed at 1:62 in the current work.

As mentioned previously, direct simulation of the system is not computationally feasible due to large number of particles involved and large size difference between carriers and drug particles. Instead, this study adopted a multi-scale approach in which simulations at different stages are performed separately. At stage I, the release of the drug particles from a single carrier particle upon impaction was modelled, aiming to establish a relationship between the release of drug particles with impact conditions (e.g. velocity, angle). Then at stage II the motions of the carrier particles in the inhaler were simulated to obtain their dynamic behaviour including collision energy information. By combining the detachment behaviour of the drug particles with the dynamics of carriers, the dispersion performance of the inhaler can then be predicted.

i). Stage I: Detachment of drug particles

In the simulations, a large carrier particle (lactose) was initially put into the center and the drug particle (mannitol) was randomly generated surrounding the carrier particle. Then the drug particle covered to the surface of carrier particle under an assumed centripetal force. The carrier-drug formulation was then put into a wall-bounded shear flow and impacted onto a target wall at a certain velocity and impact angle, as shown in Fig. 2. The amounts of powders released from the carrier, remained on the carrier surface and deposited on the wall were then analysed. It was assumed the detachment of the drug particles from the carrier surface was mainly caused by the mechanical impaction while the role of flow on powder detachment was minimum (28). Therefore, different impact velocities and angles were used while keeping the flow velocity at a constant of 20 m/s. Four simulations were carried for each condition with the agglomerate being rotated randomly to provide statistically sensible results. In total, more than 200 simulations were carried out to establish the relationship between the amount of fine particles released from the carrier and wall deposition with impact angle and velocity.

Physical Experiments

Physical experiments were performed to validate the model. In the experiments, carrier-based formulations were aerosolized using the angle throat as described in previous studies (36,37). Two angles (45° or 90°) and two flow rates (60 and 120 L/min) were selected and the tests were performed in triplicate to obtain mean values. Two polystyrene sphere carriers (Dynoseeds® TS80, TS230) had mass-median-diameter $d_{0.5}$ values of 82.8 μm (TS80) and 277.5 μm (TS230), respectively. The drug powders (salbutamol sulphate) have a median diameter of 4.2 μm. The drug was blended geometrically with the polystyrene carrier at a mass ratio of 1:50. To compare with the experimental results, simulations under similar conditions were conducted. In the simulations, the drug and carrier were Salbutamol Sulphate (4.2 μm, density 1300 kgm^{-3} and Hamaker constant 1.2×10^{-19} J) and polystyrene (density 1050 kgm^{-3} and Hamaker constant 1.0×10^{-19} J), respectively.

ii) Stage II: Dynamics of carrier particles

In the second stage, the dynamics of the carrier particles (lactose) in the inhaler was simulated. A previous study (38) has demonstrated that the dispersion of powders inside the capsule was minimal. Therefore, the discharge process from the capsule was not simulated to reduce simulation time. Instead, at the beginning of the dispersion process, a number of carrier particles

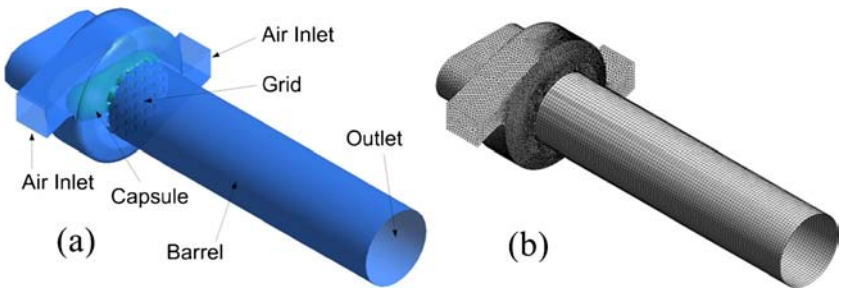

Fig. 1 (**a**) 3d view of the inhaler model; and (**b**) its grid representation.

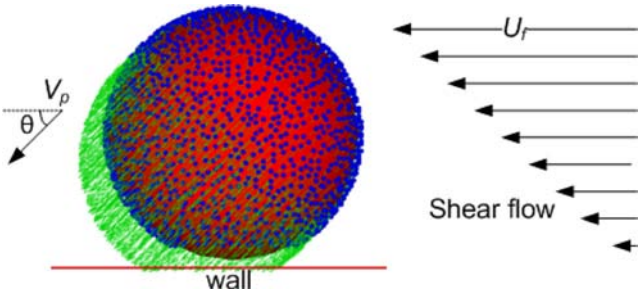

Fig. 2 Impaction of single carrier particle with a wall in a uniform shear flow.

were ejected from the two ends of the capsule into the air stream at prescribed intervals and velocities which were calculated from the spin speed of the capsule and empty time. When the carrier particles collided with each other and with the device wall, the impact information of carrier particles (e.g. collision velocity, collision angle and collision frequency) was recorded. The drug particles were not included in the simulations and they were assumed to follow the flow streamline and have no secondary breakage after being released from the carriers. For the carriers and the carrier-based agglomerate, their mass and volume differences are less than 1.5% and 1.6%, respectively. So their dynamic behaviours are almost identical. In the simulations, different sized carriers were used to investigate the effect on the inhalation performance at prescribed intervals with velocities based on the spin speed of the capsule. Different flow velocities of two air inlets from 30 to 50 m/s (equivalent to flow rates of 83 to 138 L/min) were used, which were the typical values used in physical experiments (39,40) and clinical testing (41). The spin speed of the capsule ω (rpm) was assumed to vary linearly with flow rate, Q (L/min), given by ω=45Q (42). The Dynamic Mesh Model in Fluent was adopted to model the spinning capsule. Details of the parameters used in the simulations were provided in Table 1.

Table 1 Values of the Key Parameters Used in the Simulations (43)

Parameters	Values
Diameter of carrier particles, D	70–130 μm
Diameter of drug particles, d	2 μm
Number of carrier particles, N_c	910–5830
Number of drug particles per carrier, N_d	686–4394
Density of carrier particles, ρ_c	1590 kg m^{-3}
Density of drug particles, ρ_d	1490 kg m^{-3}
Hamaker constant of carrier particles, H_{ac}	1.59×10^{-19} J
Hamaker constant of drug particles, H_{ad}	1.2×10^{-19} J
Hamaker constant of wall, H_{aw}	6.0×10^{-20} J
Single carrier impact angle, θ	15°–90°
Single carrier impact velocity, v	5–20 m/s
Shear flow velocity, u_s	20 m/s
Air flow rate , Q	82.8–138 L/min
Rotation speed of capsule, ω	3735–6210 rpm

RESULT AND DISCUSSION

Release of Drug Particles from a Single Carrier Particle

The release of drug particles from a carrier particle due to mechanical impaction was simulated under different conditions (e.g. carrier size, impaction velocity and angle). The following analysis, unless stated otherwise, is based on a carrier particle of 100 μm with an impact velocity 15 m/s and an impact angle θ=45°.

Figure 3a shows the detachment of drug particles from a carrier during the impact process. Upon impaction, drug particles are separated from the carrier particle due to the rotation and deceleration of the carrier particle. While some released particles are dispersed as aerosol, others are deposited on the wall. The particles remaining on the surface of the carrier may be further released upon next impaction.

Figure 3b shows the variations of the amount of aerosolised and deposited particles with time. It is observed the detachment of drug particles from the carrier is a very short process, all taking place within 0.1 ms. Before t=0.01 ms, the amount of particles deposited on the wall increases sharply before reaching the maximum of ~60% of total mass of the drug particles. In the meantime, the amount of drug particles released from the carrier also increases while the amount of residue on the carrier sharply decreases. Between 0.01 ms and 0.05 ms, while the wall deposition is unchanged, the amount of free powders continues to increase while the amount of particles on the carrier surface decreases. In the final stage with t>0.1 ms, both the ratios of fragments and deposition have little change, indicating the detachment process is completed. In this work, the impact is considered to finish if the particle fractions are stable more than 0.1 ms.

Aerosolisation performance depends not only on the amount of aerosol generated but also on the particle size distribution of aerosol, in particular, the aerosol of drug particles with size less than 5 μm which can be delivered into the lungs. Figure 4 shows the cumulative size distribution of aerosol at the end of impaction (t=0.1 ms). It is observed that the FPF (the mass fraction of fine particles of drug below below 5 μm) of the aerosol is about 57%. Considering the aerosol is only 31% of total mass of the drug particles, the mass fraction of fine particles in the aerosol against the total mass of drug particles (FPF_{loaded}), upon single impaction, is about 18%.

To investigate the effect of impaction parameters on the aerosolisation performance, the impact velocity and angle were varied. Figure 5 shows the fine particle fraction (FPF_{loaded}), wall deposition particle fraction (DPF_{loaded}) and carrier residue fraction (RPF_{loaded}) at the final stage under different impact conditions. As shown on Fig. 5, increasing

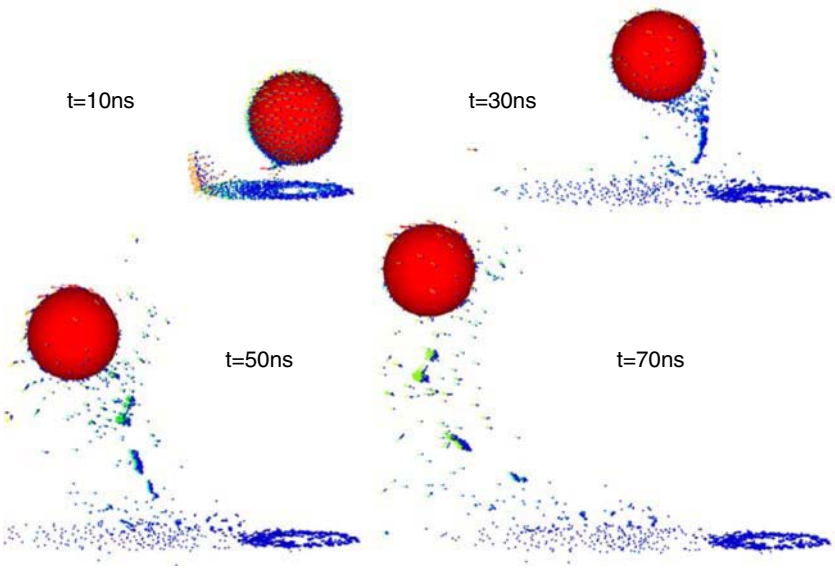

(a)

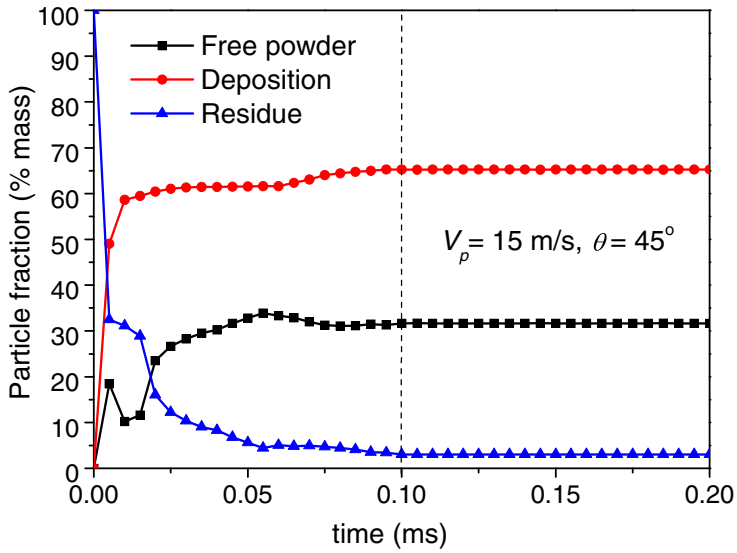

(b)

Fig. 3 (**a**) Snapshots of single carrier particle impact (diameter 100 μm) with the wall; (b) Time evolution of free drug powder fraction, wall deposition fraction and carrier residue fraction. Impact velcoity v = 15 m/s and angle θ = 45°.

impact velocity has better aerosolisation performance. For a given impact velocity, however, there exists an optimal impact angle at between 30° and 45° for maximum aerosolisation efficiency characterized by FPF_{loaded}. With increasing impact velocity and angle, RPF_{loaded} and DPF_{loaded} decreases and increases, respectively. The impact angle and velocity thus have significant effects on drug particle aerosolisation, resulting from a balance between the increased drug particles released from the carrier and increased deposition on the wall with increasing impact velocity.

The simulations model was validated by comparing the simulated fine powder fractions FPF_{loaded} with those obtained from the experiments. Figure 6 shows that the simulated results are quantitatively comparable with the experimental observations. In general, FPF_{loaded} decreases with the carrier particle size for the same impaction condition. On the other hand, FPF_{loaded} increases with impact angles and air flow rates, showing that impact angle and velocity had a significant effect on drug particle aerosolisation. The combined effects of impact velocity and impact angle on the detachment performance of the drug powders, in terms of FPF_{loaded}, RPF_{loaded} and DPF_{loaded} are shown in Fig. 7.

To quantitatively describe the effect which can be used to predict the powder dispersion in inhalers, an empirical polynomial equation was proposed, given by

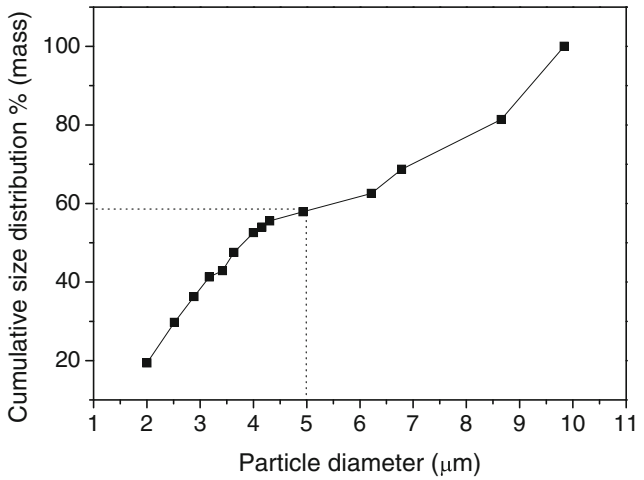

Fig. 4 Cumulative size distribution of emitted drug particles at the end of the impaction. Impact velocity v = 15 m/s and θ = 45°.

$$f(v,\theta) = a + bv + c\theta + dv^2 + e\theta^2 \quad (5)$$

Where $f(v,\theta)$ denotes FPF_{loaded}, DPF_{loaded} or RPF_{loaded} and a, b, c, d and e are fitting parameters based on the simulation results. Table 2 shows the values of the parameters for this case. Similar fittings were also obtained for other conditions. These values will be used to predict powder dispersion in inhalers.

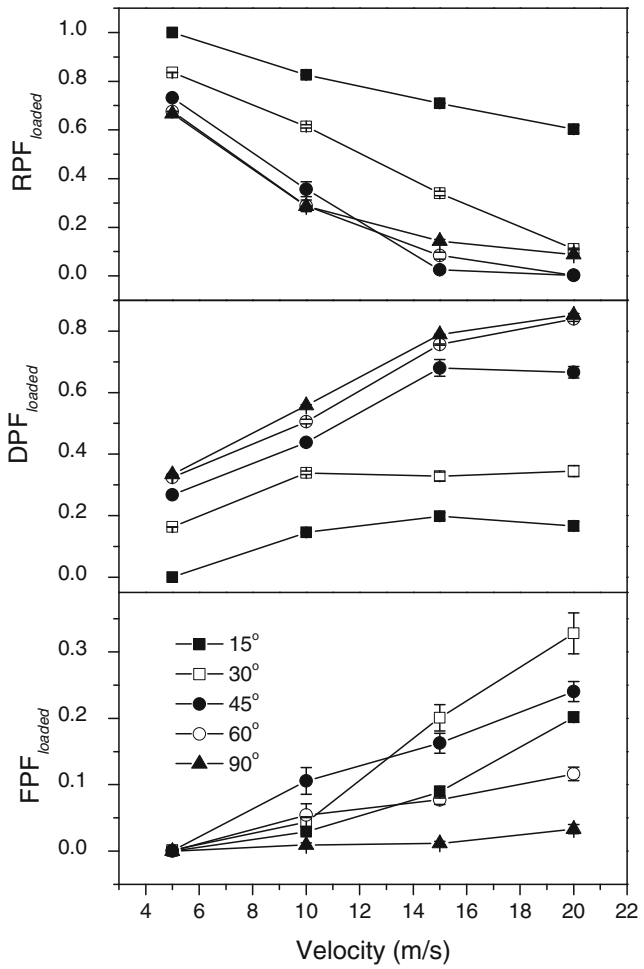

Fig. 5 Fine particle fraction (FPF_{loaded}), residual paritide fraction (RPF_{loaded}) and wall deposition particle fraction (DPF_{loaded}) with different impact velocities and angles.

Dynamics of Carrier Particles in the Inhaler

In this section, the behaviour of the carrier particles in the inhaler is discussed. While simulations with more particles can generate more accurate, they also need longer simulation time to complete. Therefore a balance approach is required in which only a minimum number of particles is simulated but the generated results, including FPF and collision energy, are independent of the number of particles in the system. Different numbers of particles ranging from 1000 to 8000 have been simulated and the results showed no significant difference, indicating the prediction is independent of the number of particles simulated. The following analysis, unless stated otherwise, is based on 1000 carrier particles of size 100 μm dispersed in the inhaler with the velocity of 40 m/s for each inlet.

In the DEM, the motions of carriers are tracked so the carrier-carrier and carrier-device collisions can be obtained separately. Figure 8a shows the spatial distributions of the carrier-device and carrier-carrier collisions in the inhaler. Most of the carrier-device collisions occur in the swirling chamber and the region with highest collision energy is located near the air inlets. Similar to the carrier-wall collisions, the vast majority of the carrier-carrier collisions also occur in the chamber. However, both the number and magnitude of the carrier-carrier collisions are much smaller than those of the carrier-wall collisions. In the barrel region, the carrier-carrier collisions are rare events (only 4~5 collisions observed in a simulation). This is because the flow in the barrel region is far less turbulent than that inside the chamber region, causing the

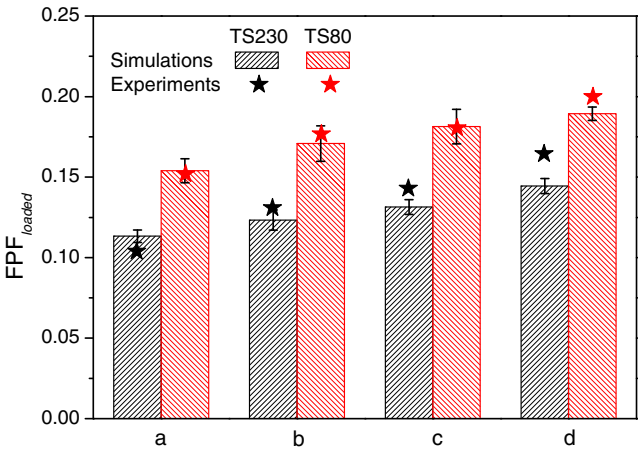

Fig. 6 FPF_{loaded} generated at different impaction angles and flow rates. (**a**) 45° and 60 L/min; (**b**) 45° and 120 L/min; (**c**) 90° and 60 L/min; and (**d**) 90° and 120 L/min. (The median sizes of TS230 and TS80 are 277.5 and 82.8 μm, respectively.)

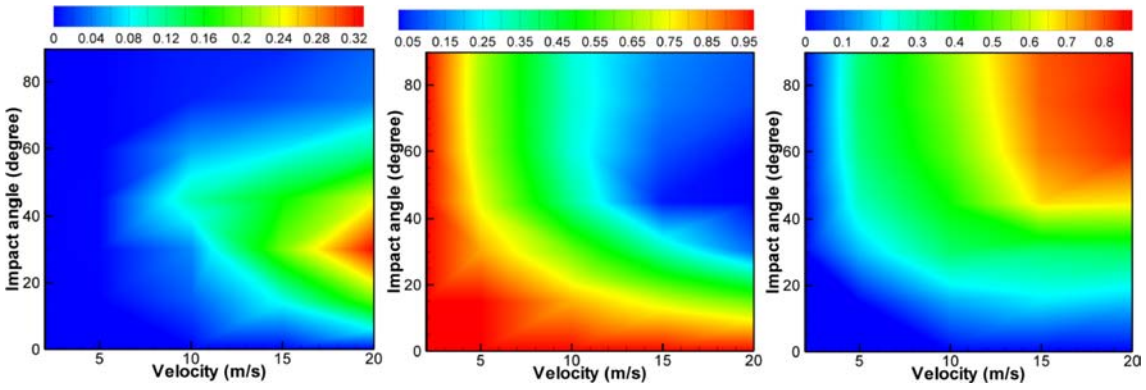

Fig. 7 Contour plots of (**a**) FPF_{loaded}, (**b**) RPF_{loaded} and (**c**) DPF_{loaded} with impact velocity and angle.

particle-particle collision less likely. Also the times entering the barrel from the chamber are different for different particles, so the concentration in the barrel region is much lower than in the chamber region, which also reduces the chance of particle-particle collisions.

Figure 8b shows that the total carrier-device collision energy is much higher (more than twenty times) than that between the carriers. There are two distinct phases during the dispersion process. From 0 to 0.85 s, the number of carrier-wall collision increases significantly while the number of the carrier-carrier collisions fluctuates at very low levels. From 0.85 s, with the carrier particles starting to exit the inhaler, the number of the carrier-device collision decreases while the number of the carrier-carrier collisions drops to almost zero.

Figure 9 shows the effect of air velocity on particle-device collision. With increasing air inlet velocity, the mean carrier-device impact velocity increases and the distribution of impact velocity becomes wider (Fig. 9a) indicating more chaotic behaviour of the carrier in the inhaler. However, the impact angle between the carriers and the device is almost unchanged with most of the impacts occurring at an angle less than 45° (Fig. 9b). Increasing air velocity also causes a decrease in the number of carrier-device impacts (Fig. 9c) as the carrier particles are more likely to follow the air flow.

Predicting Aerosolisation Performance

Once the detachment of the drug particles from the carriers under different impact conditions and the dynamics of the carrier in the inhaler are obtained, the aerosolisation performance of the inhaler can be predicted based on following assumptions:

- The drug particles are uniformly distributed at the surface of the carrier particles;
- The dynamics of the carriers are not affected by the presence of the drug particles;
- The aerosolisation performance is independent of the amount or configuration of drug particles on the carrier; and
- The aerosolisation of the drug particles is mainly caused the carrier-device mechanical impaction.

Thus the overall FPF_{loaded} of the system is given by

$$\mathrm{FPF}_{loaded} = \frac{1}{N_p}\sum_{i=1}^{N_p}\sum_{k=1}^{N_c} R_k FPF_{i,k} \tag{6}$$

where N_p is the total number of carrier particles in the inhaler, N_c is the total number of collisions for individual carrier, $FPF_{i,k}$ is the fine particle fraction in the aerosol generated from carrier particle i after the k-th collision and R_k is the fraction of drug particles remained on the carrier particle before the k-th collision ($R_1 = 1$).

Figure 10a shows the predicted FPF_{loaded} with different carrier diameters and air velocities based on Eq. 6. The results indicate that aerosolisation performance decreases with carrier size and increases with the air flow velocity, which agrees with experimental observations in the literature (15,20). Figure 10b shows the relationship

Table 2 Values of the Parameters in Eq. 5

Equation	a	b	c	d	e
FPF(v,θ)	−0.043	9.305×10^{-4}	3.72×10^{-3}	3.162×10^{-4}	-4.48×10^{-5}
RPF(v,θ)	1.592	−0.082	−0.018	1.89×10^{-3}	1.33×10^{-4}
DPF(v,θ)	−0.463	0.066	0.012	-1.71×10^{-3}	-6.71×10^{-5}

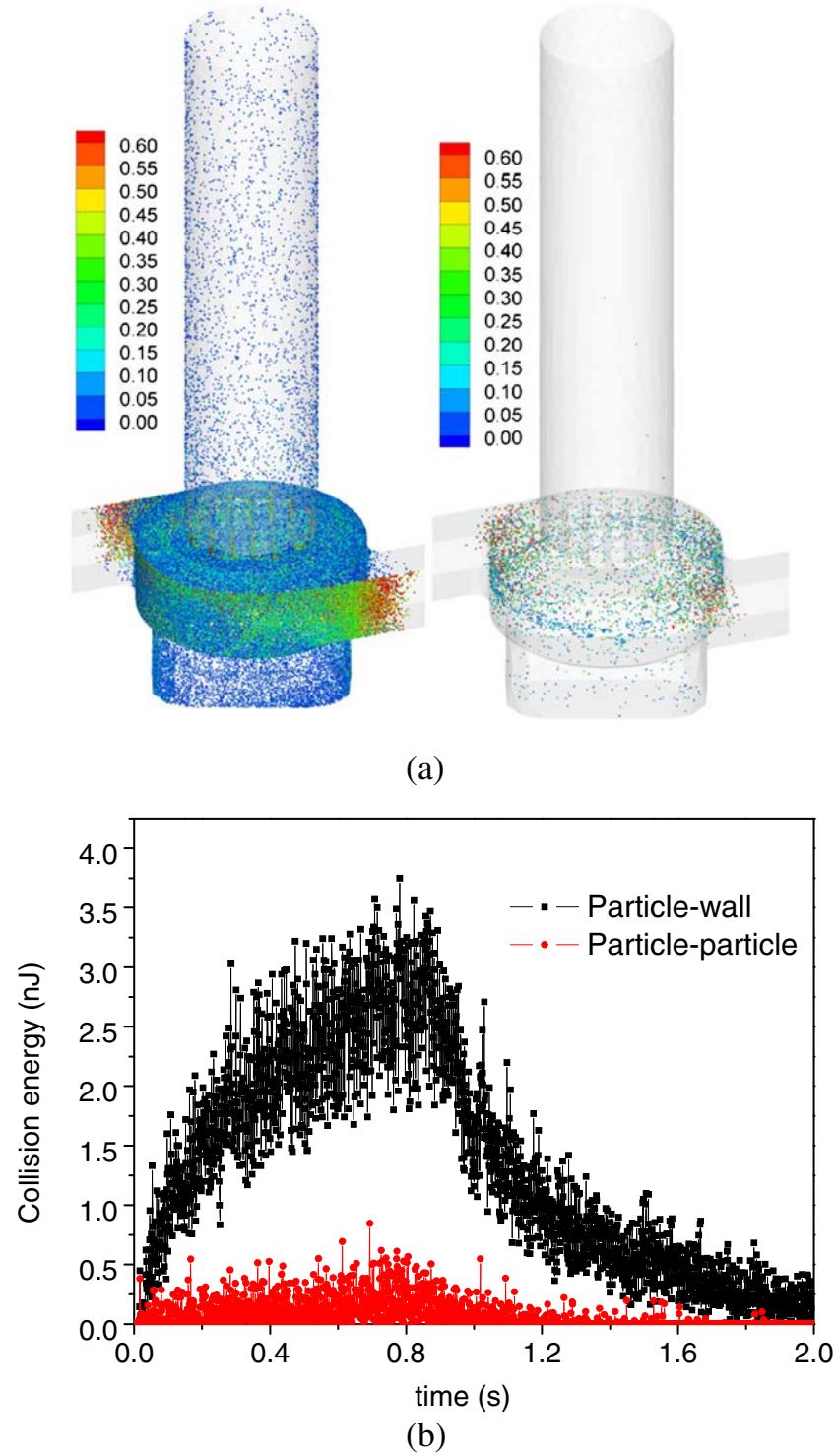

Fig. 8 (**a**) Spatial distribution of total particle-wall (*left*) and particle-particle (*right*) collision energy; (**b**) Time evaluation of particle-particle (PP) and particle-wall (PW) collision energy.

between $FPF_{emitted}$, the mass fraction of drug particles smaller than 5 μm against the total mass of emitted drug particles, and FPF_{loaded}. A linear correlation between $FPF_{emitted}$ and FPF_{loaded} suggests that the deposition particle fraction (DPF) as a whole remains a constant. This indicates that device removal efficiency is independent of carrier size and flow rate. The trend is also consistent with previous experimental observations (15,20). As increasing flow rate increases carrier-device collision intensity, so is the increase in the degree of drug liberation from the carrier surface. For a given formulation mass with a fixed carrier/drug ratio, there are more drug particles per carrier but smaller specific surface area in the large carrier system. Furthermore,

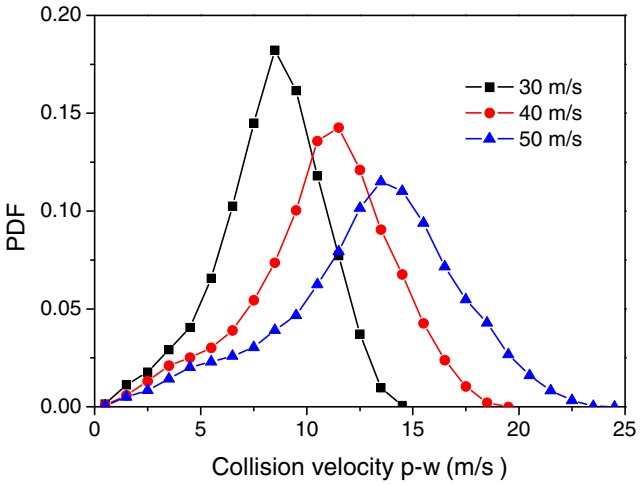

(a)

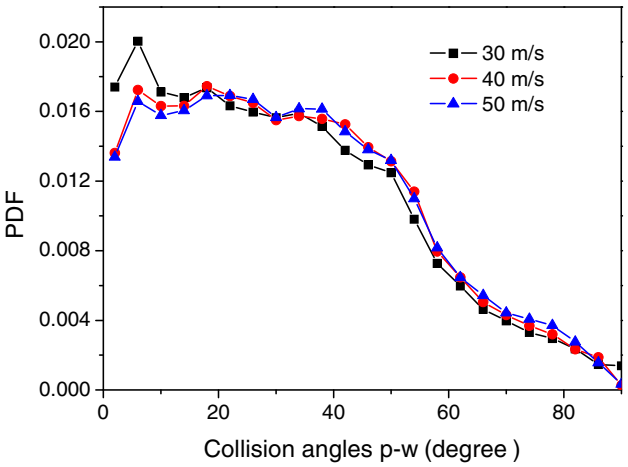

(b)

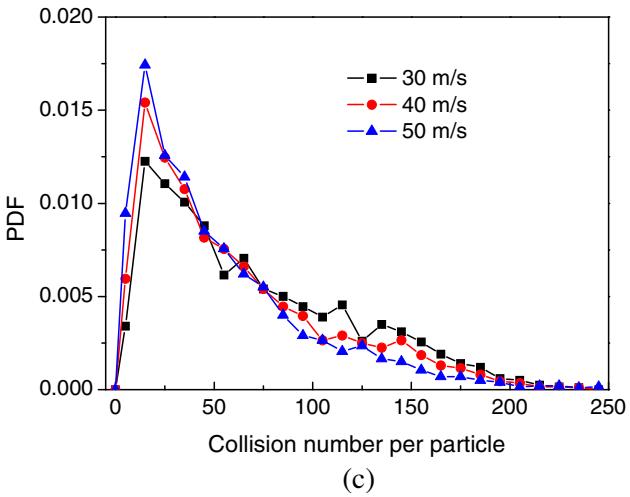

(c)

Fig. 9 The effect of air velocity on (**a**) collision velocity; (**b**) impact angle; and (**c**) the number of collisions for the carrier-device collisions.

the single carrier impaction simulations also confirm that a higher specific surface area (smaller carrier size) results in a greater probability of powder detachment.

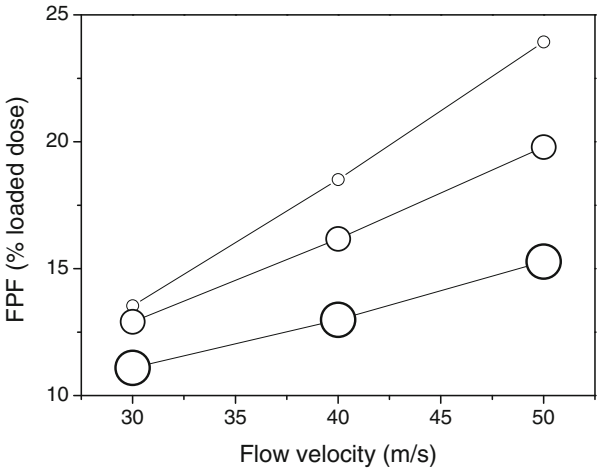

(a)

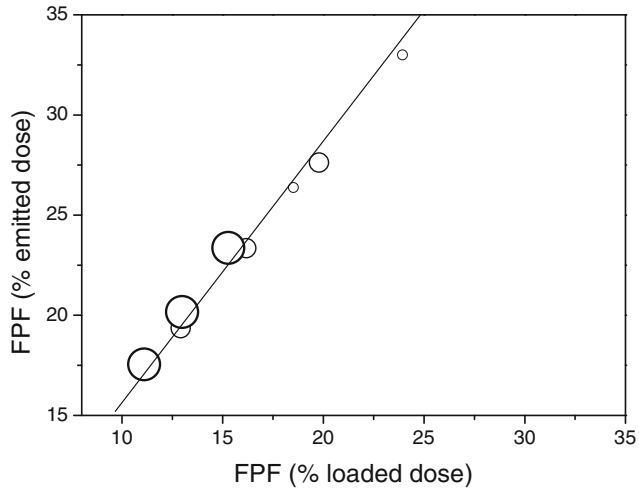

(b)

Fig. 10 (**a**) FPF_{loaded}; (**b**) relationship between $FPF_{emitted}$ and FPF_{loaded} for different sized carriers (Increasing symbol size represents increasing carrier size 70, 100 and 130 μm).

CONCLUSION

The aerosolisation process of a carrier-based dry powder inhalation system was investigated using a multi-scale approach based on the combined CFD-DEM technique. The relationship between drug particle aerosolisation and carrier particle collision was established based on single carrier impaction model. The total FPF_{loaded} was predicted by linking collisions information to drug aerosolisation by single carrier particle impaction model. The final results showed that the aerosolisation performance of carrier-based formulation decreases with the carrier particle size and increases with the air flow velocity. The numerically predicted trends of FPF_{loaded} and deposition with carrier size and air velocity are consistent

with the experimental observation. The detailed and quantitative information obtained in this study can be used to better understand the aerosolisation mechanism of carrier-based formulations.

ACKNOWLEDGMENTS AND DISCLOSURES

Authors are grateful to the Japan Society for the Promotion of Science (JSPS) and the Australia Research Council (ARC) for the financial support through the Discovery Project.

REFERENCES

1. Patton J. Breathing life into protein drugs. Nat Biotechnol. 1998;16(2):141–3.
2. Clark AR. Pulmonary delivery technology: recent advances and potential for the new millennium. In: Hickey AJ, editor. Pharmaceutical Inhalation aerosol technology. New York: Marcel Dekker, Inc.; 2004. p. 571–91.
3. Chan H-K. Dry powder aerosol drug delivery-opportunities for colloid and surface scientists. Colloids Surf A Physicochem Eng Asp. 2006;284–285:50–5.
4. Chan HK. Dry powder aerosol delivery systems: current and future research directions. J Aerosol Med-Depos Clearance Eff Lung. 2006;19(1):21–7.
5. Islam N, Gladki E. Dry powder inhalers (DPIs)–A review of device reliability and innovation. Int J Pharm. 2008;360(1–2):1–11.
6. Frijlink HW, De Boer AH. Dry powder inhalers for pulmonary drug delivery. Expert Opin Drug Deliv. 2004;1(1):67–86.
7. Bell JH, Hartley PS, Cox JS. Dry powder aerosols. I: a new powder inhalation device. J Pharm Sci. 1971;60(10):1559–64.
8. Malcolmson RJ, Embleton JK. Dry powder formulations for pulmonary delivery. Pharm Sci Technol. 1998;1(9):394–8.
9. Hersey JA. Ordered mixing: a new concept in powder mixing practice. Powder Technol. 1975;11(1):41–4.
10. Kawashima Y, Serigano T, Hino T, Yamamoto H, Takeuchi H. Effect of surface morphology of carrier lactose on dry powder inhalation property of pranlukast hydrate. Int J Pharm. 1998;172(1–2):179–88.
11. Young PM, Kwok P, Adi H, Chan HK, Traini D. Lactose composite carriers for respiratory delivery. Pharm Res. 2009;26(4):802–10.
12. Traini D, Young PM, Thielmann F, Acharya M. The influence of lactose pseudopolymorphic form on salbutamol sulfate-lactose interactions in dpi formulations. Drug Dev Ind Pharm. 2008;34(9):992–1001.
13. Dickhoff BHJ, De Boer AH, Lambregts D, Frijlink HW. The effect of carrier surface and bulk properties on drug particle detachment from crystalline lactose carrier particles during inhalation, as function of carrier payload and mixing time. Eur J Pharm Biopharm. 2003;56(2):291–302.
14. Donovan MJ, Smyth HDC. Influence of size and surface roughness of large lactose carrier particles in dry powder inhaler formulations. Int J Pharm. 2010;402(1–2):1–9.
15. Ooi J, Traini D, Hoe S, Wong W, Young PM. Does carrier size matter? A fundamental study of drug aerosolisation from carrier based dry powder inhalation systems. Int J Pharm. 2011;413(1–2):1–9.
16. Guenette E, Barrett A, Kraus D, Brody R, Harding L, Magee G. Understanding the effect of lactose particle size on the properties of DPI formulations using experimental design. Int J Pharm. 2009;380(1–2):80–8.
17. De Boer AH, Dickhoff BHJ, Hagedoorn P, Gjaltema D, Goede J, Lambregts D, *et al.* A critical evaluation of the relevant parameters for drug redispersion from adhesive mixtures during inhalation. Int J Pharm. 2005;294(1–2):173–84.
18. Islam N, Stewart P, Larson I, Hartley P. Lactose surface modification by decantation: are drug-fine lactose ratios the key to better dispersion of salmeterol xinafoate from lactose-interactive mixtures? Pharm Res. 2004;21(3):492–9.
19. Young PM, Edge S, Traini D, Jones MD, Price R, El-Sabawi D, *et al.* The influence of dose on the performance of dry powder inhalation systems. Int J Pharm. 2005;296(1–2):26–33.
20. Young PM, Wood O, Ooi J, Traini D. The influence of drug loading on formulation structure and aerosol performance in carrier based dry powder inhalers. Int J Pharm. 2011;416(1):129–35.
21. Jones MD, Price R. The influence of fine excipient particles on the performance of carrier-based dry powder inhalation formulations. Pharm Res. 2006;23(8):1665–74.
22. Hoe S, Traini D, Chan H-K, Young P. The contribution of different formulation components on the aerosol charge in carrier-based dry powder inhaler systems. Pharm Res. 2010;27(7):1325–36.
23. Young P, Sung A, Traini D, Kwok P, Chiou H, Chan H-K. Influence of humidity on the electrostatic charge and aerosol performance of dry powder inhaler carrier based systems. Pharm Res. 2007;24(5):963–70.
24. Ganderton D, Kassem, N.M. DRY Powder inhalers: Advances in Pharmaceutical Sciences. London: Academic Press; 1992. P. 165–191.
25. Coates MS, Fletcher DF, Chan HK, Raper JA. Effect of design on the performance of a dry powder inhaler using computational fluid dynamics. part 1: grid structure and mouthpiece length. J Pharm Sci. 2004;93(11):2863–76.
26. Coates MS, Chan HK, Fletcher DF, Raper JA. Effect of design on the performance of a dry powder inhaler using computational fluid dynamics. part 2: air inlet size. J Pharm Sci. 2006;95(6):1382–92.
27. Tong ZB, Yang RY, Yu AB, Adi S, Chan HK. Numerical modelling of the breakage of loose agglomerates of fine particles. Powder Technol. 2009;196(2):213–21.
28. Tong ZB, Yang RY, Chu KW, Yu AB, Adi S, Chan HK. Numerical study of the effects of particle size and polydispersity on the agglomerate dispersion in a cyclonic flow. Chem Eng J. 2010;164(2–3):432–41.
29. Tong ZB, Zheng B, Yang RY, Yu AB, Chan HK. CFD-DEM investigation of the dispersion mechanisms in commercial dry powder inhalers. Powder Technol. 2013;240:19–24.
30. Yang J, Wu C-Y, Adams M. A. three-dimensional DEM–CFD analysis of air-flow-induced detachment of api particles from carrier particles in dry powder inhalers. Acta Pharm Sinica B. 2014;4:52–9.
31. Zhu HP, Zhou ZY, Yang RY, Yu AB. Discrete particle simulation of particulate systems: theoretical developments. Chem Eng Sci. 2007;62(13):3378–96.
32. Gidaspow D. Multiphase flow and fluidization. San Diego: Academic; 1994.
33. Chu KW, Wang B, Yu AB, Vince A. Cfd-dem modelling of multiphase flow in dense medium cyclones. Powder Technol. 2009;193(3):235–47.
34. Launder BE, Reece GJ, Rodi W. Progress in development of a Reynolds-stress turbulence closure. J Fluid Mech. 1975;68:537–66.
35. Wang B, Xu DL, Chu KW, Yu AB. Numerical study of gas-solid flow in a cyclone separator. Appl Math Model. 2006;30(11):1326–42.
36. Adi S, Tong Z, Chan H-K, Yang R, Yu A. Impact angles as an alternative way to improve aerosolisation of powders for inhalation? Eur J Pharm Sci. 2010;41(2):320–7.
37. Tong Z, Adi S, Yang R, Chan H, Yu A. Numerical investigation of the de-agglomeration mechanisms of fine powders on mechanical impaction. J Aerosol Sci. 2011;42(11):811–9.

38. Coates M, Chan H-K, Fletcher D, Raper J. The role of capsule on the performance of a dry powder inhaler using computational and experimental analyses. Pharm Res. 2005;22(6):923–32.
39. Chew NYK, Bagster DF, Chan HK. Effect of particle size, air flow and inhaler device on the aerosolisation of disodium cromoglycate powders. Int J Pharm. 2000;206(1–2):75–83.
40. Chew NYK, Chan HK. Influence of particle size, air flow, and inhaler device on the dispersion of mannitol powders as aerosols. Pharm Res. 1999;16(7):1098–103.
41. Bronsky EA, Grossman J, Henis MJ, Gallo PP, Yegen Ü, Cioppa GD, *et al.* Inspiratory flow rates and volumes with the Aerolizer dry powder inhaler in asthmatic children and adults. Curr Med Res Opin. 2004;20(2):131–7.
42. Coates MS, Chan HK, Fletcher DF, Raper JA. Influence of air flow on the performance of a dry powder inhaler using computational and experimental analyses. Pharm Res. 2005;22(9):1445–53.
43. Tong Z, Yang R, Yu A, Adi S, Chan H. Numerical modelling of the breakage of loose agglomerates of fine particles. Powder Technol. 2009;196(2):213–21.